Theoretical investigation of the Ar+H 2 + (0v4, j=0)→ ArH + +H nonadiabatic reaction dynamics

F. Aguillon and M. Sizun

Citation: The Journal of Chemical Physics **106**, 9551 (1997); doi: 10.1063/1.473856
View online: http://dx.doi.org/10.1063/1.473856
View Table of Contents: http://scitation.aip.org/content/aip/journal/jcp/106/23?ver=pdfcov
Published by the AIP Publishing

Theoretical investigation of the $Ar+H_2^+(0\leqslant v\leqslant 4, j=0)\rightarrow ArH^++H$ nonadiabatic reaction dynamics

F. Aguillon and M. Sizun
Laboratoire des Collisions Atomiques et Moléculaires, URA du CNRS n°281, Bâtiment 351, Université Paris XI, 91405 Orsay cedex, France

(Received 22 January 1997; accepted 12 March 1997)

The title reaction is investigated using a semiclassical coupled wave packet method where the hyperspherical radius ρ is treated classically and the other coordinates quantally. Dynamical calculations are performed in a coplanarlike approximation using eight coupled electronic states. State-to-state reaction cross sections are obtained in the energy range $0.3\ \text{eV}\leqslant E_{\text{coll}}\leqslant 5\ \text{eV}$ for five different initial rovibrational states. The internal energy of the ArH^+ product is found to be very high, especially at low collision energy. A comprehensive analysis of the reaction mechanisms is presented. © *1997 American Institute of Physics.* [S0021-9606(97)01423-2]

I. INTRODUCTION

The present paper is devoted to the study of the reaction

$$Ar+H_2^+(v)\rightarrow ArH^++H. \tag{1}$$

The first experimental results concerning this reaction appeared almost 30 years ago.[1] Since that time, detailed experimental information has been obtained, especially on the differential cross sections[2] and v-dependence of the total cross sections.[3–5] Although there is no measurement of the ArH^+ internal state distribution, there is an experimental indication that this product is very hot.[2]

Theoretical investigations of reaction (1) have been performed using a number of approximations: restriction to the collinear geometry,[6] trajectory surface hopping (TSH) approximation,[7] and infinite order sudden (IOS) approximation.[8,9] An exact calculation restricted to the zero angular momentum case has recently been published.[10] Most of these theoretical studies[6–9] have been made in conjunction with the study of the other reaction involving the (ArH_2^+) system:

$$Ar^++H_2\rightarrow ArH^++H. \tag{2}$$

Recently, a semiclassical coupled wave packet method has been used to study the latter reaction.[11,12] The work presented here is essentially an extension of this work to reaction (1). The same DIMZO (diatomics in molecule with zero overlap) potential energy surfaces[13] have been used. Dynamical calculations have been performed using the semiclassical hyperspherical coupled wave packet method developed by Billing and co-workers.[14] In this method, the hyperspherical radius is treated classically, and the other nuclear degrees of freedom are treated quantally using a numerical representation over a grid. Compared to the TSH method,[7] the advantage of this technique is that quantal nonadiabatic effects accompanying the reaction are treated exactly. Compared to the IOS methods,[8,9] its advantage is to take into account the changes in the orientation of the molecule occurring during the collision; these orientation effects have been shown to play an important role in reaction (2). Finally, this method makes it possible to obtain state-to-state cross sections.

The time dependent treatment inherent to the semiclassical wave packet approach provides a sensible picture of the reaction by allowing one to visualize the intimate collision mechanisms. This property will be used to extract simple models that help to in understanding what happens during the collision. We shall in particular address the following questions:

(i) What is the role of the nonadiabatic transitions in this reaction?
(ii) What is the influence of the initial vibrational state on this exothermic reaction?
(iii) Which are the reaction mechanisms?

The method used is summarized in Sec. II; the results are presented and compared to previously published data in Sec. III. Finally, Sec. IV is devoted to a thorough discussion of the mechanisms involved in the reaction.

II. METHOD

The method has been presented in detail in previous publications,[11,12] and will only be briefly summarized here.

The potential energy matrix is determined in three steps. *First*, a DIMZO calculation similar to that of Kuntz *et al.*[13] is performed to compute the potential energy matrix regardless of the spin orbit coupling. This step concerns 28 states correlated to Ar^++H_2 and $Ar+H_2^+$, where H_2 and H_2^+ are either in their ground gerade state, or in the first dissociative ungerade state. *Second*, the spin orbit interaction is introduced in a way similar to the method proposed by Tully.[15] Among the above mentioned 28 states, 12 correspond to quartet states and are disregarded. The neglect of the quartet states has been shown to be a very good approximation for the Ar^++H_2 systems.[11] Only the remaining 16 doublet states of the ArH_2^+ system are considered in the following. *Third*, these states are symmetrized in such a way that the potential energy matrix U has the block-diagonal form

TABLE I. Labeling of the diabatic states used in the calculation. m_s is the projection of the spin angular momentum of H_2^+ onto the Ar–H_2 axis. J is the total electronic angular momentum of the Ar^+ ion, and M_J its projection along the same axis.

Short name	Expression
$Ar+H_2^+$	$\frac{1}{\sqrt{2}}[Ar\,H_{2g}^+](\|m_s=1/2\rangle - i\|m_s=-1/2\rangle)$
$Ar^+(3/2,1/2)+H_2$	$\frac{1}{\sqrt{2}}[Ar^+H_{2g}](\|J=3/2,\ M_J=1/2\rangle - i\|J=3/2,M_J=-1/2\rangle)$
$Ar^+(1/2)+H_2$	$1\sqrt{2}\,[Ar+H2g](\|J=1/2,\ MJ=1/2\rangle + i\|J=1/2,M_J=-1/2\rangle)$

$$U=\begin{pmatrix} V & 0 \\ 0 & V^* \end{pmatrix}, \tag{3}$$

where V is an 8×8 complex hermitian matrix. This symmetrization significantly reduces the bulk of the calculations; the price to pay for it is that (i) the potential energy matrix elements are complex and (ii) the labeling of the electronic diabatic states ζ_n is somewhat complicated.[12] So, as shown in Table I, we have assigned short names to the electronic basis states we will have to refer to in the discussion. The asymptotic potential energy curves are presented in Fig. 1. Two important features of this figure are worth stressing:

(i) In the entrance channel, the $Ar^+ + H_2$ and the $Ar+H_2^+$ curves cross. This makes the adiabatic approximation problematic for systems whose wave function extends on both sides of the crossing point;

(ii) In the product channel, all the states are dissociative, except the ground state of ArH^+.

The two lowest adiabatic potential energy surfaces (PES) in collinear geometry are presented in Fig. 2. One can see on this figure that the ground adiabatic PES, which is the only reactive one, is very far energetically from all other PES except at the large intermolecular distance in the entrance valley, where nonadiabatic transitions will occur.

In the dynamical calculations, we use a slightly modified version[14] of Johnson's hyperspherical coordinates.[16] Three Euler angles α, β, and γ define the orientation of the triatomic plane; the triatomic triangle is described by the hyperspherical radius ρ and two hyperangles $0\leqslant\theta\leqslant\pi/2$ and $0\leqslant\varphi\leqslant 2\pi$. In a given arrangement channel c, the relationships between the hyperspherical coordinates and Jacobi coordinates r_c, R_c, and $\eta_c\in[0,\pi]$ are:

$$\frac{r_c^2}{d_c^2}=\frac{\rho^2}{2}\,(1-\sin\,\theta\,\cos(\varphi-\varphi_c)), \tag{4}$$

$$d_c^2R_c^2=\frac{\rho^2}{2}\,(1+\sin\,\theta\,\cos(\varphi-\varphi_c)), \tag{5}$$

$$\cos\,\eta_c=\frac{\sin\,\theta\,\sin(\varphi-\varphi_c)}{\sqrt{1-\sin^2\theta\,\cos^2(\varphi-\varphi_c)}}. \tag{6}$$

In the following, the channel $c=1$ will refer to the $Ar+H_2$ channel, and channels $c=2$ and $c=3$ to the two ArH+H channels. d_c and φ_c depend only on the mass m_1 of the Ar atom, and m_2 and m_3 of the H atoms:

$$d_c=\sqrt{\frac{m_c}{\mu}\left(1-\frac{m_c}{m_1+m_2+m_3}\right)} \tag{7}$$

and

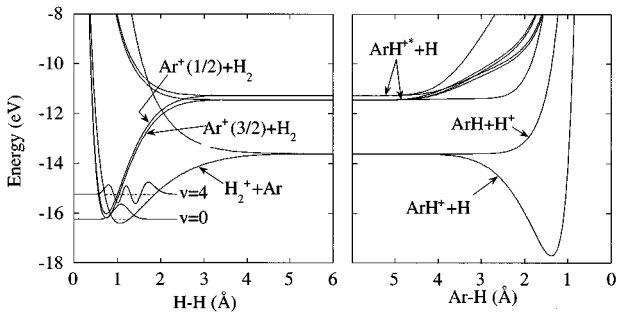

FIG. 1. Asymptotic potential energy curves of the ArH_2^+ system. The $v=0$ and $v=4$ H_2^+ wave functions are represented in the H_2^+ well.

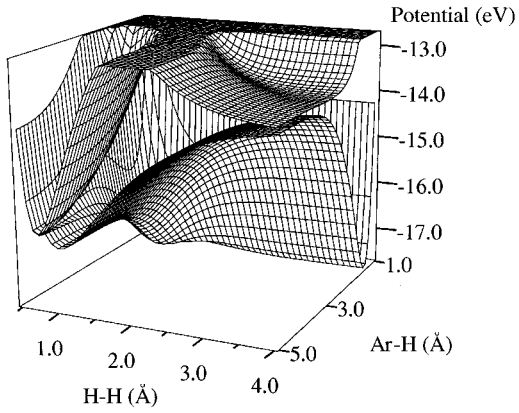

FIG. 2. Lowest adiabatic DIMZO potential energy surfaces of the ArH_2^+ system in collinear geometry.

$$\varphi_1=\pi, \quad \varphi_2=\pi+2\tan^{-1}\left(\frac{m_3}{\mu}\right),$$

$$\varphi_3=\pi-2\tan^{-1}\left(\frac{m_2}{\mu}\right), \tag{8}$$

μ is the hyperspherical reduced mass:

$$\mu=\sqrt{\frac{m_1m_2m_3}{m_1+m_2+m_3}}. \tag{9}$$

Two approximations are made to reduce the amount of computation. First, the coplanar approximation[17] consists of retaining only one partial wave for each value of the total angular momentum $\mathscr{J}$ for the description of the time evolution of the external coordinates α, β, and γ. Second, the motion along the ρ coordinate is handled classically, while the motions along the θ and φ are handled quantally. The internal coordinates of the system are then described by one classical trajectory $\rho(t)$ and eight 2D coupled wave packets $\Psi_n(\theta,\varphi,t)$ associated with the respective electronic diabatic states ζ_n. The volume element related to the wave function is simply $d\theta\, d\varphi$. The time evolution of Ψ_n obeys a set of coupled partial differential equations:

$$i\hbar\,\frac{\partial\Psi_n}{\partial t}=T_n\Psi_n+\sum_{n'}\,V_{nn'}(\theta,\varphi,\rho)\Psi_{n'}, \tag{10}$$

where the kinetic energy operator is[16c]

$$T_n=\frac{\hbar^2}{2\mu\rho^2}\left(-4\,\frac{\partial^2}{\partial\theta^2}+\frac{1}{\sin^2\,\theta}\left(-4\,\frac{\partial^2}{\partial\varphi^2}+4i\mathscr{J}\cos\,\theta\,\frac{\partial}{\partial\varphi}+\mathscr{J}^2\right)-\left(\frac{1}{4}+\frac{4}{\sin^2\,2\theta}\right)\right). \tag{11}$$

The $V_{nn'}$ are the potential energy matrix elements of the 8×8 V matrix defined in Eq. (3). Both T_n and $V_{nn'}$ depend on the time through the classical variable $\rho(t)$. The semiclassical energy conserving trajectory method[18] (SCECT) provides the $\rho(t)$ evolution as the solution of the classical Hamilton equations involving the Hamiltonian $H_{\rm cl}$

$$H_{\rm cl}=\frac{P_\rho^2}{2\mu}+\sum_n\,\langle\Psi_n|T_n|\Psi_n\rangle+\sum_{n,n'}\,\langle\Psi_n|V_{nn'}|\Psi_{n'}\rangle, \tag{12}$$

where the integration is carried out over the θ and φ coordinates. This SCECT method has been used in all cases except $v=2$. Indeed, because the $Ar+H_2^+(v=2)$ state is energetically very close to the $Ar^+(1/2)+H_2$ initial state, there is a strong coupling between the vibrational motion, which is handled quantally, and the collision motion, which is handled classically. This is a situation where the SCECT approximation fails. In order to fix this problem, a ''forced trajectory'' $\rho(t)$ has been used, compelled to be the same as that of the $Ar^+(3/2,\,1/2)+H_2$ initial state. Such a procedure has been justified and successfully applied in Ref. 12 for the resonant $Ar^+(1/2)+H_2$ state.

In the asymptotic regions ($\rho\to\infty$), unless the collision leads to complete dissociation, an eigenstate of the system is characterized by:

(i) the total energy, which is a constant of motion;
(ii) the electronic state n;
(iii) the arrangement channel c;
(iv) the vibrational quantum number v of the diatomic molecule;
(v) the rotational quantum numbers $\mathscr{J}$, $\mathscr{M}$, j, and l.[19] The total angular momentum $\mathscr{J}$ and its projection $\mathscr{M}$ along a fixed direction, are constants of motion. j is the rotational quantum number of the diatomic molecule, and l is the orbital angular momentum associated with the relative atom–molecule motion.

Such an asymptotic state is usually described using the Jacobi coordinates R_c, r_c, and η_c for the arrangement channel c. The correspondence between the Jacobi semiclassical description, where R_c is treated classically, and the hyperspherical semiclassical description, where ρ is treated classically, is[12,20]

$$\rho=d_cR_c \tag{13}$$

for the classical quantities, and

$$\Psi^\infty(\theta,\varphi)=\sqrt{\frac{\pi d_c^4}{2}}\sqrt{\frac{2l+1}{2\mathscr{J}+1}}\times R_c\,\frac{g_v(r_c)}{\sqrt{r_c}}\sum_\mu\,(i)^\mu\langle jl\mu0|\mathscr{J}\mu\rangle\times\mathscr{d}^{\mathscr{J}}_{\mathscr{M}\mu}(\pi/2)\sqrt{\sin\,\eta_c}Y_{j\mu}(\eta_c,0) \tag{14}$$

for the wave functions. In the above expression, g_v is a vibrational eigenstate, $Y_{j\mu}$ a spherical harmonic, and $\mathscr{d}^{\mathscr{J}}_{\mathscr{M}\mu}$ is a Wigner matrix.[21]

Each of the coupled wave packets $\Psi_n(\theta,\varphi)$ is represented on an equally spaced rectangular mesh, having 256 points in φ and 64 points in θ. The initial wave packet is prepared according to Eq. (14). The initial value of ρ is 10 Å, and the initial value of P_ρ is determined by the center of mass collision energy $E_{\rm coll}$ and the total angular momentum $\mathscr{J}$.[12] The integration of the time dependent Schrödinger equation makes use of the FFT[22] technique to evaluate the Hamiltonian and of the Lanczos[23] algorithm to obtain a compact form of the time evolution operator at each time step. At the end of the collision, the wave packet is analyzed. When state integrated information is looked for, a rough analysis is performed by defining three zones[14c] of the grid (θ,φ), each one associated with a given channel, and by integrating the $|\Psi_n(\theta,\varphi;\rho)|^2$ probability density in these zones to obtain the reaction probability. When state-to-state probabilities are required, the final wave packets are analyzed by projecting them onto asymptotic rovibrational wave functions constructed from Eq. (14). Calculations have been carried out in the energy range 0.3 to 5 eV, for the five states of H_2^+ ($0\leqslant v\leqslant 4$, $j=0$). Since the reaction probability depends slowly on the total angular momentum, about ten values of $\mathscr{J}$ were found sufficient to obtain accurate enough cross sections.

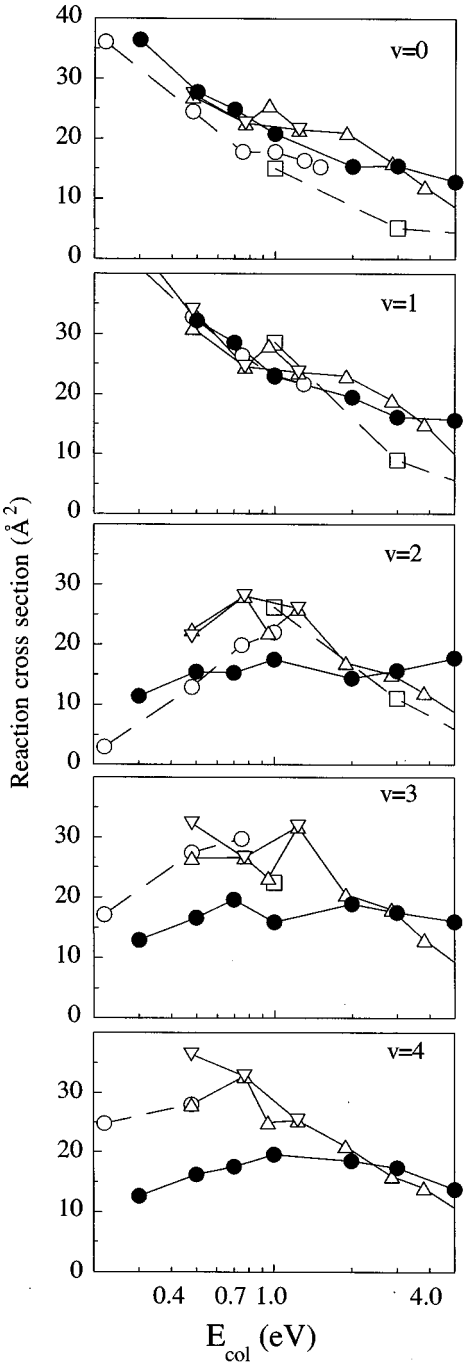

FIG. 3. Absolute cross sections for the reaction $Ar+H_2^+(v)\rightarrow ArH^++H$. Experimental results: downward triangles, Ref. 3; upward triangles, Ref. 5. Theoretical results: squares, Ref. 7; open circles, Ref. 9(a); closed circles, present work.

III. RESULTS

The v dependent total cross sections as a function of the collision energy $E_{\rm coll}$ are shown in Fig. 3. It is convenient in the discussion to distinguish between two different groups of vibrational levels. The $v=0$ and $v=1$ reaction cross sections decrease with the collision energy. For these two vibrational levels, the agreement between experimental and theoretical results is good. The $v=2$ to $v=4$ levels do not exhibit a monotonic decrease of the reaction cross section with collision energy; besides, the agreement between theoretical results and experiments is not as good as for the first group.

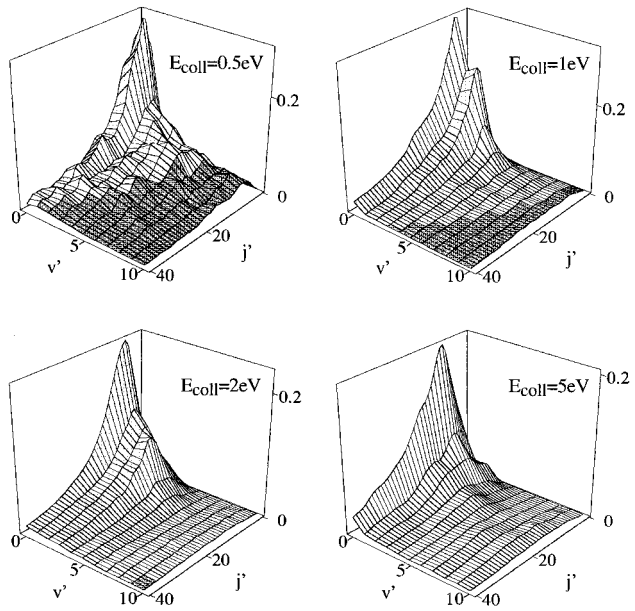

FIG. 4. Rovibrational state-to-state cross sections (in Å^2) for the production of $ArH^+(v',j')$ from the reaction $Ar+H_2^+(v=0,\ j=0)$ as a function of the center of mass collision energy $E_{\rm coll}$. The grey zones correspond to closed channels, where the cross sections should vanish.

Two examples of state-to-state results are presented in Figs. 4 and 5, which show an important vibrational and rotational excitation of the ArH^+ product. This strong excita-

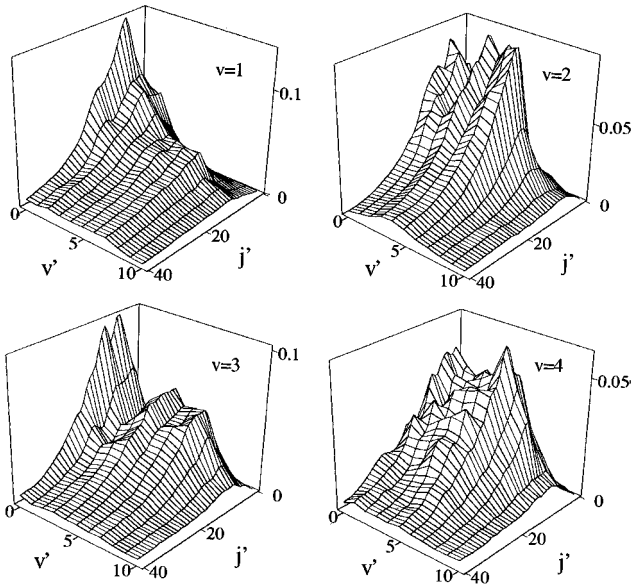

FIG. 5. Rovibrational state-to-state cross sections (in Å^2) for the production of $ArH^+(v',j')$ from the reaction $Ar+H_2^+(v,j=0)$ as a function of the initial vibrational state v at a collision energy $E_{\rm coll}$=5.0 eV. The $v=0$ situation is shown in Fig. 4.

tion is in agreement with the experimental data of Bilotta *et al.*,[2] who have measured a significant production of ''superexcited'' ArH^+ molecules. The TSH calculations[7] lead to the same amount of average vibrational excitation, while the rotational excitation is even higher. Finally, the exact calculation of Gilibert *et al.*[10] also predicts a strong internal excitation of the ArH^+ molecules produced in the $\mathscr{J}=0$ collisions, especially in the rotational degree of freedom. Unfortunately, these exact results have been obtained at very low collision energy (below 0.1 eV), where the semiclassical approximation is believed to be unreliable. An interesting and unexpected feature can be observed in Fig. 4: the vibrational excitation of the ArH^+ product is larger as the collision energy decreases. This feature is observed independently of the initial quantum vibrational number v. It will be shown in the next section that it is related to the different mechanisms that take place at high or low collision energy. Another evidence of energy dependent mechanisms has also been observed experimentally:[2] above $E_{\mathrm{coll}}=1$ eV, the angular distribution of the ArH^+ molecule is strongly peaked in the backward direction with respect to the H_2^+ incident direction. Below 1 eV the angular distribution is very broad.

One has to note in Fig. 4 a significant population of closed channels at low collision energy. This well-known drawback of the semiclassical methods[24] is very perceptible in the present case, since all of the electronic energy released by this exothermic reaction ($\Delta E=1.3$ eV) is finally found in the internal ArH^+ degrees of freedom, as already observed both experimentally[2] and theoretically.[7] Then, at low collision energy, the average quantal energy at the end of the collision is almost equal to the total available energy; this is the situation where closed channels are most likely to be populated by semiclassical methods. Population of closed channels may also occur in some specific situations as a result of numerical artifacts. Indeed, in order to limit the amount of computation, we have fixed the grid stepsizes $\delta\theta$ and $\delta\varphi$ to a relatively large value. As the distances related to $\delta\theta$ and $\delta\varphi$ are $\rho\delta\theta$ and $\rho\delta\varphi$, respectively, they become large at the end of the collision. Then, when highly excited ArH^+ states are actually produced, these stepsizes become too large to represent accurately the rovibrational distribution. Because of these two effects, the vibronic populations at the end of the collision can only be considered as qualitative at low energy.

IV. DISCUSSION

As in the $Ar^+ + H_2$ reactive collisions, the reaction (1) can be described as a two-step process. *First*, the nonadiabatic transitions take place at large intermolecular distances. *Second*, the reaction takes place in a purely adiabatic regime. This two-step mechanism can be related to the adiabatic PES shown in Fig. 2, keeping in mind that the ground adiabatic PES is the only reactive one. Soon in the entrance valley, the energy gap between the ground PES and the first excited PES becomes so large that nonadiabatic transitions involving the ground adiabatic state cannot occur anymore at the collision energies studied here. An illustration of this two-step mechanism is given in Fig. 6. At $t\approx 40$ fs, the ground adiabatic state becomes decoupled. The reaction itself occurs between $t\approx 60$ fs and $t\approx 90$ fs on the ground adiabatic PES. After $t\approx 90$ fs, the evolution of the ArH^+ product also takes place on the ground adiabatic PES only.

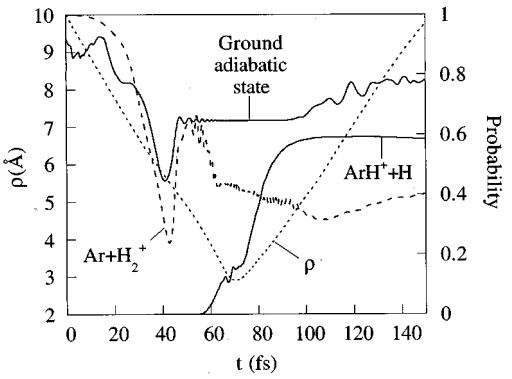

FIG. 6. History of the investigated nonadiabatic reaction. The figure shows the time evolution of the hyperradius ρ, the initial diabatic electronic state population, the adiabatic electronic ground state population, and the population in the ArH^+ channel. The collision energy is $E=0.7$ eV and the total angular momentum is $\mathscr{J}=50$. The initial state is $Ar+H_2^+(v=2)$.

This qualitative description is confirmed quantitatively in the following way. The dynamical calculation is performed using eight diabatic electronic coupled wave packets during the first stage of the collision. As soon as the system behaves adiabatically, i.e., as soon as the adiabatic ground state population is constant, the diabatic calculation is stopped, and the ground adiabatic electronic wave packet $\psi_g^{(a)}$ is extracted from the diabatic wave packets ψ_n according to

$$\psi_g^{(a)}(\theta,\varphi)=\sum_n \psi_n(\theta,\varphi)\langle\xi_g|\zeta_n\rangle, \tag{15}$$

where ξ_g is the ground adiabatic electronic state. Finally, $\psi_g^{(a)}$ is propagated on the ground adiabatic PES. This calculation is in excellent agreement with the fully diabatic calculation as far as the ArH^+ channel is concerned. One should emphasize that the *diabatic* part of the calculation that is carried out first is necessary to describe precisely the reaction dynamics. This is obvious for the high v levels, since the crossing point between $Ar^+ + H_2$ and the $Ar+H_2^+$ curves lies in the classically allowed region. This is also the case even for the $v=0$ case, because the vibrational wave function does not vanish at the crossing point, although this point lies in the classically forbidden region (Fig. 1). In that sense, the $Ar+H_2^+$ reaction cannot be regarded as a purely adiabatic process.

The two-step character of the reaction greatly simplifies the interpretation of the dynamics. Indeed, it is not necessary to take the reactive channels into account during the first step, which involves coupled electronic states. Conversely, the reaction takes place in a single decoupled electronic state. In the following, we shall examine successively these two steps.

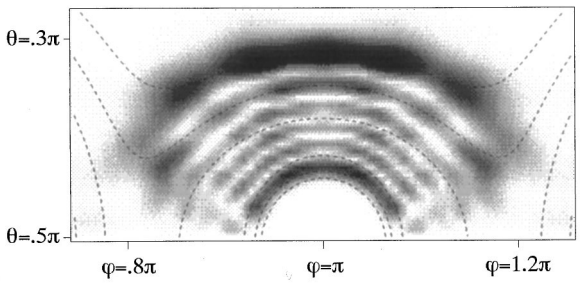

FIG. 7. Adiabatic ground state probability density. The system is initially in the $Ar+H_2^+(v=4)$ state; the collision energy is $E=0.5$ eV, and the total angular momentum is $\mathscr{J}=0$. The picture is drawn in the incoming stage of the collision, for $\rho=4.4$ Å, corresponding approximately to the end of the first step of the reaction. At this point, 83% of the initial wave packet is in the ground adiabatic electronic state. The remaining 17% are in excited adiabatic electronic states. In the hyperspherical view displayed here, the point $r_{H-H}=0$ corresponds to $\theta=\pi/2$ and $\varphi=\pi$; along radial lines issued from this point, the r_{H-H} distance increases, while the H_2 molecule does not rotate; conversely, along circles centered on the same point, the H_2 molecule rotates with a constant r_{H-H} elongation. The radial structure shows that the system is in its $v=5$ vibrational level. The absence of any clear angular structure shows that the orientation of the H_2 axis is roughly isotropic, just like the one prepared at the beginning of the collision.

A. First step: Nonadiabatic transitions

This first step describes the time evolution of the system until its behavior becomes adiabatic. As an example, this first step ends at $t \approx 50$ fs in the case illustrated in Fig. 6. In order to understand the reaction dynamics, one has to consider the following question: what is at the end of this first step—the *adiabatic* rovibronic state of the hydrogen molecule when the system is initially prepared in a given *diabatic* $Ar+H_2^+(v)$ state? The answer is found in the analysis of the ground adiabatic wave packet, as defined in Eq. (15), at the end of the first step. As an example, for the $Ar+H_2^+(v=4)$, $E_{coll}=5$ eV reaction, this analysis shows that:

(i) the squared norm of this wave packet is 0.83; the remaining 17% of the system is electronically excited in the adiabatic view, and does not react;
(ii) the wave packet exhibits a nice $v=5$ vibrational structure, as seen in Fig. 7;
(iii) there is almost no rotational structure, as seen in the same figure.

In the energy range studied here, the latter point is a general rule. On the other hand, at the end of the first step, both the norm of the ground adiabatic electronic state and the vibrational structure of the system in this electronic state strongly depend on the initial vibrational state of H_2^+, as displayed in Table II. Simple pictures provide an explanation of this behavior.

Time scale considerations explain the rotational behavior of the system in the first stage of the collision. Indeed, the rotational period of H_2^+ in a superposition of $j=0$ and $j=1$ state is 87 fs. That is in most cases longer than the total duration of the first step, and always much longer than the time it takes for the coupling to become large and anisotropic enough to induce rotational excitation. Then, the distribution of orientations of the H_2 axis at the end of the first step is about the same as at the beginning of the collision, i.e., almost uniform.

TABLE II. Example of the dependence of the population in the ground adiabatic electronic state at the turning point versus the initial v quantum number of H_2^+, when the collision energy is 0.5 eV, and the total angular momentum is $\mathscr{J}=30$. The ground adiabatic state is mainly found in the vibrational state indicated in the third column at the end of the first part of the collision.

Initial vibrational quantum number	Ground adiabatic state population at the turning point	Vibrational quantum number in the ground adiabatic electronic state
4	83%	5
3	95%	4
2	48%	3
1	99%	1
0	99.9%	0

A sudden approximation is not relevant to explain the vibronic behavior of the system, which can be understood using an adiabatic vibronic network.[12] To build this network, only the three states that play a role at this stage of the collision need to be taken into account: the initial $Ar+H_2^+(v)$ state, and two charge exchange states with which the initial state is coupled, namely the $Ar^+(3/2,1/2)+H_2(v)$ state and the $Ar^+(1/2)+H_2(v)$ state. At the large internuclear distances considered here, it appears that this network does not depend much on the orientation of the H–H axis. So the network displayed in Fig. 8, which has been obtained in the collinear configuration, is representative of all orientations. Such a network can be used as a correlation diagram. Indeed, the adiabatic vibronic states have the following properties:

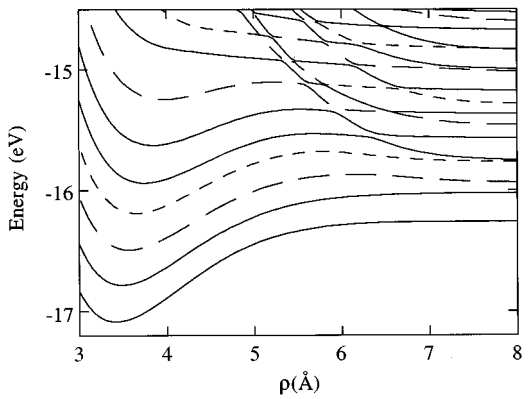

FIG. 8. Adiabatic hyperspherical vibronic network obtained in collinear configuration; only the $Ar-H_2$ reactant-like states have been taken into account. At large ρ, these vibronic states are correlated with the $Ar+H_2^+(^2\Sigma_g)$ channel (full lines), the $Ar^+(3/2,1/2)+H_2$ channel (long dashes), and to the $Ar^+(1/2)+H_2$ channel (short dashes). At short distances, these adiabatic vibronic states are correlated with vibrational eigenstates of the electronic adiabatic states. The neglect of the ArH–H reactive-like states makes this vibronic network inadequate at short ρ: it can be used for qualitative purposes only to describe the beginning of the collision process.

(i) they are vibrational eigenstates of the *diabatic* electronic states at very low coupling, i.e., at large intermolecular distance;
(ii) they are vibrational eigenstates of the *adiabatic* electronic states at very large coupling, i.e., at small intermolecular distance.

The $Ar+H_2^+(v=0)$ and $(v=1)$ initial states are found at the end of the first step of the collision in the ground electronic state, and in the vibrational states $v=0$ and $v=1$, respectively (Table II). This has to be related to the fact that the corresponding vibronic states are well separated from all other levels in the vibronic network (Fig. 8). So their vibronic behavior is strictly adiabatic in the energy range studied here. The $Ar+H_2^+(v\geqslant 2)$ initial states are not entirely found at the end of the first step of the collision in the ground electronic state (Table II). Figure 8 suggests that two types of nonadiabatic transitions can take place:

(i) *first*, the weakly avoided crossings can be traversed diabatically. The wave packet calculations indicate that the behavior of the system in the region of these weakly avoided crossings is almost perfectly diabatic at the highest collision energy studied here, and become less diabatic below 1 eV. This is the reason why the reactive cross sections of the $(v=3)$ and the $(v=4)$ initial states decrease as the collision energy decreases (Fig. 3). Indeed, these two initial states have to traverse diabatically such weakly avoided crossings in order to reach the $(v=4)$ and $(v=5)$ vibrational levels of the reactive adiabatic PES;
(ii) *second*, as the $Ar+H_2^+(v=2)$ and $Ar^+(1/2)+H_2$ $(v=0)$ are asymptotically in close resonance, Demkov-type transitions can occur at very large intermolecular distance ($\rho\approx 8$ Å) between these two levels. So, the interpretation of the $(v=2)$ results of Table II is that this level is correlated through a Demkov-type transition to the $(v=3)$ level of the ground adiabatic electronic state, and through multiple Landau–Zener-type transitions to an excited adiabatic electronic state.

One should note that the same procedure also applies to the interpretation of the $Ar^+(J)+H_2(v)$ reactions;[12] by the way, vibronic effects for these reactions are even more spectacular, preliminary calculations show that the $Ar^+(J)+H_2$ $(v=1)$ is nonreactive, while the $Ar^+(J)+H_2(v=0)$ states strongly react.

B. Second step: Reaction

The analysis of the time evolution of the coupled wave packets shows that the reaction mechanisms depend on both the collision energy E_{coll} and the initial vibrational quantum number v of H_2^+. These dependences are due to purely dynamical effects. Indeed, all reactions take place on the ground adiabatic potential energy surface, whose most important features are as follows:

(i) the collinear geometry plays a central role: the saddle point between the $Ar+H_2^+$ valley and the ArH^++H valley is reached in that collinear geometry. Moreover, it is energetically favored in the entrance valley, except at small intermolecular distances, where steric effects are more important in collinear geometry than in perpendicular geometry;
(ii) the potential is strongly attractive ($\sim$1.2 eV) in the entrance valley, and almost flat in the product valley (Figs. 2 and 9).

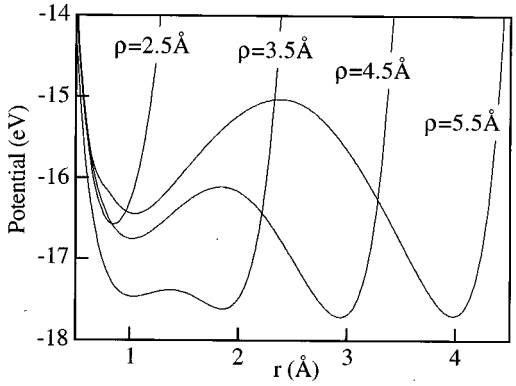

FIG. 9. Cuts of the ground adiabatic PES in collinear geometry. Each curve is obtained at a fixed value of the hyperradius ρ. r is the H–H bond distance: the left well is the $Ar+H_2^+$ well, the right one is the ArH^++H well.

As the reactive collisions take place in the *decoupled* adiabatic ground state, the time evolution of the ground adiabatic wavepacket $\psi_g^{(a)}$, as defined in Eq. (15), will be monitored to provide the interpretation of the dynamical effects. In the following, four typical situations will be presented successively ($E_{\mathrm{coll}}=5$ eV, $v=0$), ($E_{\mathrm{coll}}=5$ eV, $v=4$), ($E_{\mathrm{coll}}=0.3$ eV, $v=4$), ($E_{\mathrm{coll}}=0.3$ eV, $v=0$). For each of these four cases, we will analyze the time evolution of a

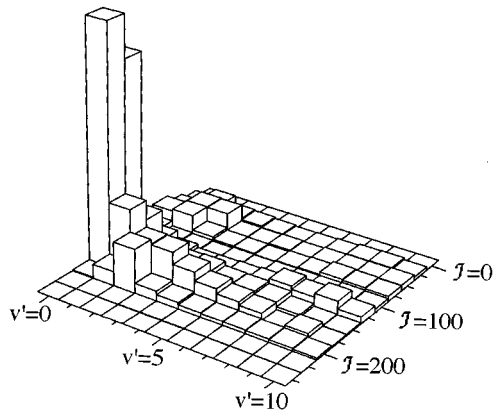

FIG. 10. Contribution of the different values of the total angular momentum $\mathcal{J}$ to the vibrational state-to-state cross sections for reaction $Ar+H_2^+(v=0)\rightarrow ArH^+(v')+H$ at a collision energy $E_{\mathrm{coll}}=5$ eV.

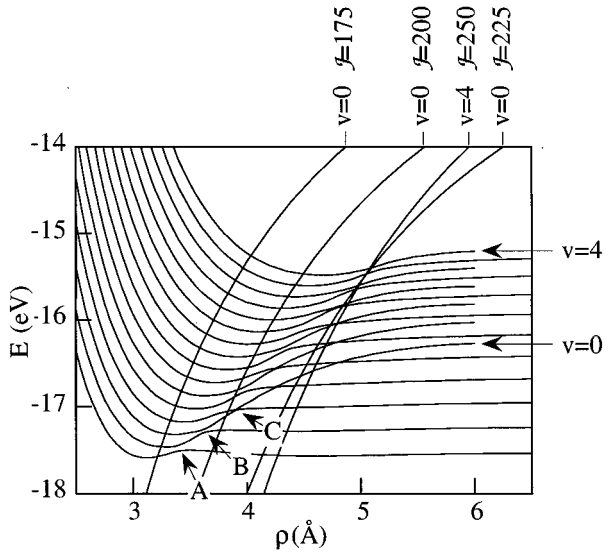

FIG. 11. Adiabatic hyperspherical vibronic network obtained in collinear geometry; only the ground adiabatic electronic state is considered. The states drawn up to $\rho=6.5$ Å can be asymptotically identified as $ArH^+(v)$ + H states. Those drawn up to $\rho=6$ Å are correlated with reagent channel states. The arrows $v=0$ and $v=4$ do not indicate the actual vibrational quantum numbers of the adiabatic PES, but the levels that are correlated during the first step of the collision with the entrance states $Ar+H_2^+$ (v=0) and ($v=4$). Four curves represent the total energy for a $Ar+H_2^+(v)$, $E_{coll}=5$ eV collision minus the $\mathscr{J}$ dependent centrifugal energy, and hence indicate the position of the turning point for each vibrational level.

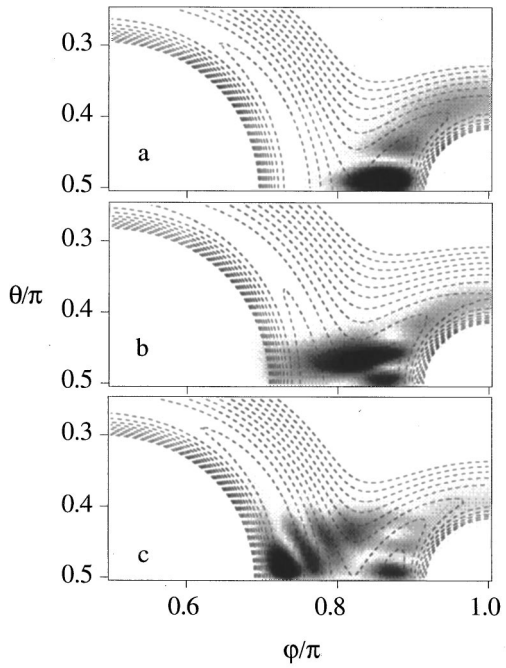

FIG. 12. Time evolution of the adiabatic ground state probability density. The initial conditions are: $Ar+H_2^+(v=0)$ state, $E_{coll}=5$ eV, $\mathscr{J}=175$. The density and the potential are drawn only in one-eighth $\pi\geqslant\varphi\geqslant\pi/2$, $\pi/2\geqslant\theta\geqslant\pi/4$ of the total hyperangular range. At $\varphi=\pi$, $\theta=\pi/2$, the distance H–H is zero: at $\varphi\approx\pi/2$, $\theta=\pi/2$, Ar–H=0. The dashed contour lines represent the ground adiabatic potential; the energy gap between two successive lines is 0.1 eV. In frame a, the hyperradius is $\rho=3.59$ Å; the wave packet is still in the $Ar–H_2^+$ valley. 4 fs later (frame b), when the turning point is reached ($\rho=\rho_T=3.39$ Å), the potential barrier between the two valleys wears away; the wave packet can then enter the product region. 8 fs later (frame c), $\rho=3.67$ Å, and the wave packet is split up into two parts by the potential ridge; the main part of it is in the ArH^+ valley, near the bottom of this valley.

significant collision, i.e., the collision associated with the angular momentum $\mathscr{J}$ which contributes at most to the total cross sections.

1. High collision energy: Low vibrational excitation

The prototype case of that section is $v=0$ and $E_{coll}=5$ eV. The state-to-state cross sections for this case show a weak vibrational excitation and a strong rotational excitation (Fig. 4). Figure 10 presents the contributions of the different $\mathscr{J}$ values to the vibrational cross sections: $\mathscr{J}=175$ and $\mathscr{J}=150$ give by far the main contribution, mainly on the $v'=0$ state; $\mathscr{J}=200$ gives a small contribution peaked on the $v'=2$ state. To interpret these results, we consider a different vibrational network (Fig. 11) than that discussed in Sec. IV A. Only the vibrational eigenstates of the ground adiabatic electronic state in collinear geometry are considered in its construction. A number of avoided crossings between the $Ar+H_2^+$ manifold and the ArH^++H manifold can be observed in this network. For $E_{coll}=5$ eV, the behavior of the system for large ρ is strictly diabatic at these crossings. On the other hand, for small ρ, transitions can occur at the avoided crossing labeled A and B in Fig. 11, giving rise to $ArH^+(v'=0)$ and to $ArH^+(v'=1)$, respectively. Somewhat weaker transitions at the avoided crossing C also occur, giving rise to $ArH^+(v'=2)$. Centrifugal effects govern the minimal value ρ_T reached by the system: for $\mathscr{J}>200$, the crossing point C is not reached, and there is no reaction. At $\mathscr{J}=200$, this weakly reactive crossing point C produces a small amount of $ArH^+(v=2)$ molecules. At $\mathscr{J}=175$, the reactive crossing points A and B produce a large amount of $ArH^+(v=0$ and 1) molecules.

The associated reaction mechanism is suggested by Fig. 9: at $\rho\approx3.5$ Å, the kinetic energy of the wave packet located in the H_2^+ well becomes larger than the ridge separating the H_2^+ and ArH^+ valleys. Then, the wave packet can smoothly slip in the ArH^+ valley. The exact $\mathscr{J}=175$ result of Fig. 12 confirms this very simple interpretation:

(i) first, one can note that the reaction takes place near the collinear geometry $\theta=\pi/2$;
(ii) second, the reaction is due to the lowering of the barrier during a time interval that is just sufficient to let the wave packet react. In the following, such a smooth mechanism will be referred to as an abstraction mechanism;
(iii) third, this reaction does not produce any significant vibrational excitation, since the bottoms of the H_2^+ and ArH^+ valleys have about the same energy when the reaction takes place.

The $\mathscr{J}=200$ reaction is seen in Fig. 10 to be less reactive but to produce more vibrational excitation of the products. In the

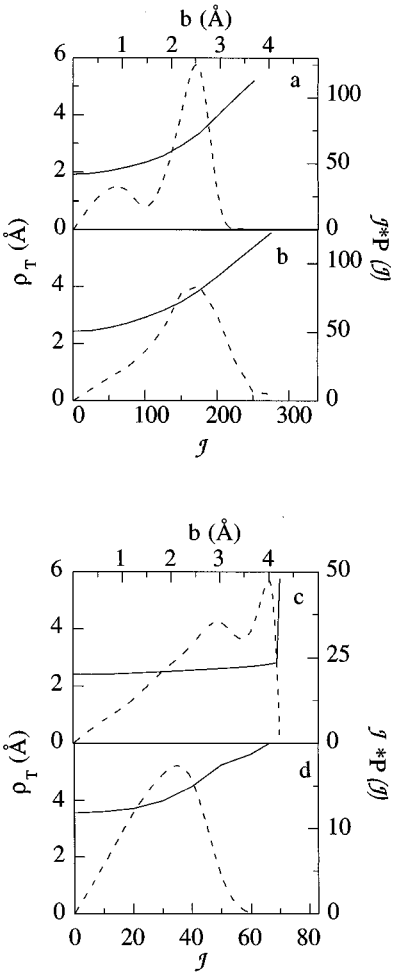

FIG. 13. Values of the turning point hyperradius ρ_T (full lines) and reaction probability (dashed lines), versus the impact parameter b or the total angular momentum $\mathscr{J}$. The collision energy E_{coll} and the initial H_2^+ vibrational quantum number v are as follows: frame a: $E_{\text{coll}}=5$ eV, $v=0$; frame b: $E_{\text{coll}}=5$ eV, $v=4$; frame c: $E_{\text{coll}}=0.3$ eV, $v=0$; frame d: $E_{\text{coll}}=0.3$ eV, $v=4$.

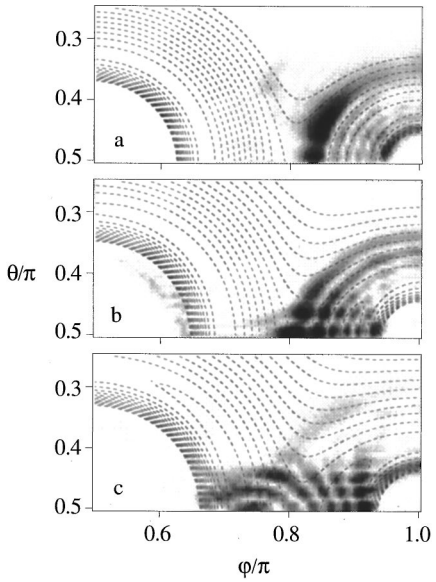

FIG. 14. Adiabatic ground state probability density corresponding to the following initial conditions: $Ar+H_2^+(v=4)$ state, $E_{\text{coll}}=5$ eV, $\mathscr{J}=175$. The dashed contour lines represent the ground adiabatic potential; the energy gap between two successive lines is 0.2 eV. Frame (a) is recorded at $t=-10$ fs, i.e., 10 fs before the turning point is reached. It corresponds to $\rho=5.0$ Å, which is approximately the position where the potential barrier between the two valleys becomes lower than the energy of the wave packet. Frame (b) is recorded at $t=-6$ fs and $\rho=4.3$ Å. Frame (c) is recorded at $t=-2$ fs and $\rho=3.9$ Å.

wave packet view, this has to be related to the insufficient lowering of the ridge, which makes the reaction more difficult. It is noteworthy that when this $\mathscr{J}=200$ reaction takes place, the energy of the H_2^+ valley is higher than that of the ArH^+ one, thereby leading to vibrational excitation of the ArH^+ product. For $\mathscr{J}<150$, the system can overcome the ridge before the turning point. The wave packet can then oscillate between the two valleys; this is reflected in the oscillation displayed in Fig. 13(a).

The abstraction mechanism that dominates the high collision energy process also explains the large rotational energy of the ArH^+ product. Indeed, this abstraction mechanism can be roughly described as follows: near the turning point, the inner H atom of the collinear $(Ar–H–H)^+$ molecule is attached to the Ar atom, without changing its velocity. Then its angular momentum, which represents a substantial part of the initial orbital angular momentum, is transformed into an ArH^+ rotation angular momentum.

2. High collision energy; high vibrational excitation

The prototype case of that section is $v=4$ and $E_{\text{coll}}=5$ eV. The vibronic network of Fig. 11, used in the same way as in the previous section, predicts a prominent contribution of $\mathscr{J}=250$ to the reaction cross section, which would lead to the formation of the ArH^+ products in the vibrational level $v'=9$. Figures 5 and 13(b) show that this prediction is wrong; the reason for that inconsistency is the large number of avoided reactive crossings available to the system: unlike the $v=0$ case, the system can perform a large number of nonadiabatic vibronic transitions. The complex dynamics of these collisions is better understood using a wave packet description. The reaction is still governed by an abstraction mechanism. Differences with the previous situation ($E_{\text{coll}}=5$ eV, $v=0$) are that (i) the wave packet is broader and (ii) the vibrational energy of the system is about 1 eV larger. This vibrational energy helps the system to overcome the potential barrier between the reagent and the product valley (Fig. 9). The reaction can thus take place at larger ρ value. As a consequence, the reaction can occur at $\mathscr{J}$ values as high as 250. Nevertheless, at such a high $\mathscr{J}$ value, the so-called ''potential opening time,'' i.e., the time interval during which the potential barrier can be overcome, is short. Only the part of the wave packet located nearest to the ridge can react. When $\mathscr{J}$ decreases, ρ_T decreases, and the ''potential opening time'' increases, thereby enhancing the reaction probability. When $\mathscr{J}$ reaches values below 150, a new phenomenon appears: the system oscillates in the ArH^+ valley, and goes back in the reagent valley during the opening time.

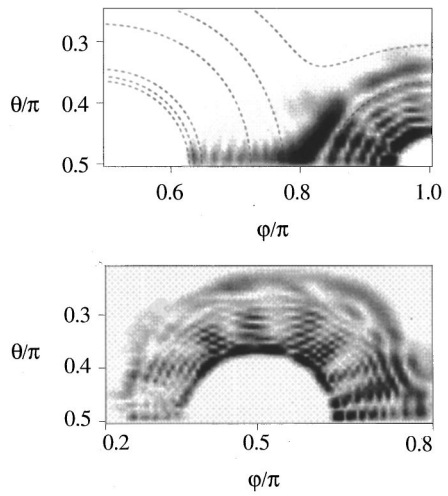

FIG. 15. Adiabatic ground state probability density corresponding to the following initial conditions: $Ar+H_2^+(v=4)$ state, $E_{coll}=0.3$ eV, $\mathscr{J}=40$. The upper frame is recorded at $t=-16$ fs, i.e., 16 fs before the turning point is reached. It corresponds to $\rho=4.7$ Å. One can note that a highly excited vibrational structure of the collinear ArH_2^+ molecule has already developed. The dashed contour lines represent the ground adiabatic potential; the energy gap between two successive lines is 1 eV. The lower frame shows highly vibrationally excited ArH^+ state at $t=34$ fs, at $\rho=5.13$ Å.

Then the reaction probability reaches a maximum at $\mathscr{J}=150$. The main contribution to the cross section is due to $\mathscr{J}=175$ [Fig. 13(b)], which can be regarded as a typical $\mathscr{J}$ value for the formation of ArH^+ from $H_2^+(v=4)$ at $E_{coll}=5$ eV.

For the latter $\mathscr{J}=175$, the turning point is reached about 10 fs after the opening of the potential barrier. Figure 14 shows that during these 10 fs, only about one-half of the wave packet has the time to move to the ArH^+ valley: the reaction takes place in a range of ρ values. It is clear from Fig. 9 that the ArH^+ vibrational energy is higher when the system overcomes the potential barrier at large ρ than at small ρ, because in these cases both the bottom of the H_2^+ valley and the potential barrier are energetically higher than the bottom of the ArH^+ valley. The above explains why the $E_{coll}=5$ eV, $v=4$, $\mathscr{J}=175$ reaction exhibits a broad vibrational distribution of the products below the $v'=9$ level corresponding to the largest possible reactive ρ value. This is consistent with the observed state-to-state reaction cross section (Fig. 5).

3. Low collision energy; high vibrational excitation

The prototype case of this section is $v=4$ and $E_{coll}=0.3$ eV. The internal energy of the ArH^+ product is paradoxically larger at this low collision energy than that found at $E_{coll}=5$ eV. Moreover, although the reactive PES is strongly attractive in the entrance valley (Figs. 2 and 9), the turning point value is larger at low energy than at high energy (Fig. 13), as would be the case with a repulsive PES.

In the present case the ''potential opening time'' is very long (typically 50 fs) compared to characteristic vibrational times. Three stages can be distinguished during this time interval. During the first stage, a linear ArH_2^+ state builds (Fig. 15). If the collision energy were zero, transitions between the two valleys could occur at large ρ by tunnelling through the potential barrier. In such a tunnelling situation, only vibrational levels of $H+ArH^+$ energetically resonant with the incoming $Ar+H_2^+$ state would be populated. At $E_{coll}=0.3$ eV, reaction actually occurs both by tunnelling through the barrier and by moving slightly over the barrier. The resonance condition still holds, although not strictly anymore. It leads to the formation of a collinear ArH_2^+ characterized by very high vibrational quantum numbers (Fig. 15). During the second stage, the populated ArH_2^+ state has a vibrationally adiabatic evolution. When ρ decreases, the ArH_2^+ well shrinks (Fig. 9), and the energy of the high lying vibrational ArH_2^+ states becomes very large. Then, despite the attractive shape of the electronic PES, the high lying vibronic potentials are repulsive: this is the reason why the turning point value ρ_T is actually so large [Fig. 13(d)]. The third stage takes place near the end of the reaction, when the $ArH^+ + H$ valley and the $Ar+H_2^+$ valley move away from each other. The same resonance arguments as those put forward above can be invoked to explain that the ArH^+ vibrational levels that are populated are those that are energetically resonant with the ArH_2^+ populated state, i.e., with the initial $Ar+H_2^+$ state. This is clearly observed in Fig. 15, where the vibrational structure of ArH^+ looks almost like a $v'=9$ structure, as predicted by a resonance condition (Fig. 11).

4. Low collision energy; low vibrational excitation

The prototype case of this section is $v=0$ and $E_{coll}=0.3$ eV. This collision regime is quite different from all previous situations. This is witnessed by the opacity function and the $\mathscr{J}$ dependence of the hyperradius at the turning point ρ_T [Fig. 13(c)]. It is seen that as long as $\mathscr{J}<70$, the reaction probability and ρ_T are nearly constant; then, at $\mathscr{J}=70$, the reaction probability suddenly vanishes while the ρ_T increases from 2.8 to 5.8 Å. The nonreactivity and the large distance of closest approach ρ_T are closely related; indeed, in the collinear vibronic network shown in Fig. 11, the reactive crossings (denoted A, B, and C) involved in this reaction are located at ρ smaller than 4 Å. At $\mathscr{J}\geqslant 70$, the centrifugal barrier is sufficient to prevent the system reaching the inner reactive zone. Conversely, for all $\mathscr{J}<70$, the system reaches small ρ attractive regions, where the centrifugal energy is much smaller than the depth of the attractive well. Hence, the distance of closest approach, and more generally speaking the reaction mechanism, do not depend on the value of $\mathscr{J}$ as soon as $\mathscr{J}<70$. The small distance of closest approach observed at low energy is consistent with the measured differential cross sections,[2] which show a broad angular diffusion range at low energy, in contrast with the strong backward scattering of ArH^+ with respect to the incident Ar^+ direction observed at high energy.

Reactive $E_{coll}=0.3$ eV, $v=0$ collisions are all characterized by the important role of the orientation effects.[11] Indeed, at small ρ values such as those reached in these collisions, steric effects tend to favor the perpendicular geometry with

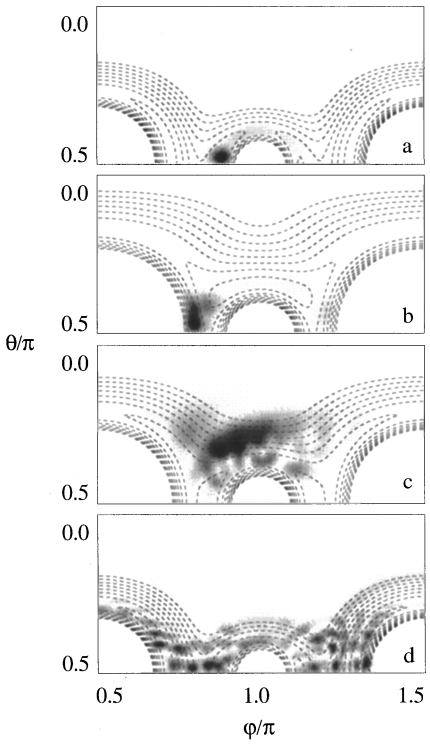

FIG. 16. Adiabatic ground state probability density as a function of time. The initial conditions are: $Ar+H_2^+(v=0)$ state, $E_{coll}=0.3$ eV, $\mathscr{J}=50$. The dashed contour lines represent the ground adiabatic potential; the energy gap between two successive lines is 0.2 eV. The frame (a) shows the wave packet at $\rho=3.82$ Å, $t=-11$ fs, i.e., 11 fs before the turning point is reached. Frame (b): $\rho=2.69$ Å, $t=-1$ fs. Frame (c): $\rho=3.07$ Å, $t=9$ fs. Frame (d): $\rho=4.01$ Å, $t=29$ fs.

respect to the collinear geometry. Then, the history of the collision, as displayed in Fig. 16 for $\mathscr{J}=50$, is very close to that observed in the $Ar^+ + H_2$ collisions.[11] The wave packet is still in collinear configuration 10 fs before the turning point is reached; near the turning point, the wave packet has moved to the $Ar–H^+$ valley, and the Ar–H bond is very compressed. From that point, two different mechanisms can be observed. For the main part of the wave packet, the potential energy of the compressed Ar–H bond is transferred to the rotation of H_2. The H_2 molecule turns by 180°, and forms the ArH^+ molecule with the opposite H atom, in the so-called pop-out mechanism. The rest of the wave packet simply escapes in the nearest ArH^+ valley, leading to a direct mechanism. Besides, it is observed that the mentioned mechanisms lead to different internal energies of the ArH^+ product: the pop-out mechanism produces higher internal energy than the direct mechanism does. As in a previously analyzed $Ar^+(J=3/2)+H_2(v=0)$, $E_{coll}=0.3$ eV reaction,[11] this phenomenon is probably related to the fact that the potential energy stored in the Ar–H bond during the compression stage is not the same for the whole wave packet. The part of the wave packet that is strongly compressed gains a lot of internal energy from the collisional motion, giving rise to the fierce pop-out mechanism. Conversely, for the part of the wave packet that does not experience any strong compression, the energy transfer between collisional motion and internal motion is weak. In that case, the mechanism is not very different from the abstraction mechanism observed for the $E_{coll}=5$ eV, $v=0$ case.

V. CONCLUSION

The first state-to-state cross sections have been obtained for the title reaction in the 0.3 to 5 eV energy range. Total reaction cross sections are in good agreement with previously published experimental and theoretical data. State-to-state cross sections show a large amount of vibrational and rotational excitation; an unexpected feature of the internal energy distribution is that the excitation of ArH^+ product is higher at low collision energy than at high collision energy.

A careful analysis of the wave packets as the reaction goes on has been presented. We have shown that the $Ar+H_2^+$ reaction can be seen as a two-step process. The first step is the sharing of the system between the adiabatic electronic states. During this step, the electric charge, which was initially located on H_2^+, is shared between the three atoms. Such an electronic rearrangement also occurs in the entrance stage of the $Ar^+ + H_2$ collision. In that sense, the nonadiabatic $Ar^+ + H_2$ reaction as well as the $Ar+H_2^+$ one, which is occasionally presented as an adiabatic reaction, are very similar; they both involve charge transfer during their first step. The second step is the reaction itself, which takes place uniquely on the decoupled ArH_2^+ adiabatic ground state. It thus involves only the part of the system that is left at the end of the first step in the ground adiabatic electronic state. The reactivity of this part of the system is controlled by the opening of a potential barrier between the reagent valley and the product valley. Time scale considerations between this opening time and the time the system spends to explore the two valleys, on one hand, and the vibrational state of the system at the beginning of the second step, on the other hand, explain the wealth of the dynamical effects observed in the various conditions studied.

The present work makes use of a few approximations, which restrict its validity to the energy range studied here. On the one hand, the common trajectory semiclassical approximation is expected to be less and less reliable when the collision energy decreases. On the other hand, the coplanar approximation is probably a source of overestimation of the high energy cross section. Indeed, this approximation tends to overestimate the weight of the reactive collinear configurations occurring during the collision.[12] Nevertheless, our description of the reaction mechanism can be extended outside the energy range studied here. At higher energy, several effects account for the decrease of the reaction cross section. It has to be related to the decrease of the ''potential opening time,'' which has to be at least of the order of a vibrational period of H_2^+ or ArH^+ in order to let the system react, and to the fact that the ArH^+ rotational energy increases as the collision energy increases, and tends to become larger than the ArH^+ dissociation energy. At very low energy, the reaction mechanism itself, i.e., the second step of the collision, probably becomes independent of the collision energy; indeed, the system experiences a strongly attractive electronic poten-

tial (more than 1 eV) before the reaction itself. Then, once the system has reached the inner region, which at low collision energy can only occur if the system is in the attractive ground adiabatic state, its reaction probability does not depend on its collision energy. The only dependence then occurs during the first step of the collision, which determines the probability the system has to reach the inner region. This is the reason for the success of capture models in the determination of the total cross sections. For the $v=0$ and 1 state, the reaction probability is approximately constant at low energy, and the cross section increases with decreasing collision energy. For $v \geqslant 2$, the behavior of this probability is certainly much more complicated, because there is a large number of rovibronic transitions that can occur at large distances between the $Ar+H_2^+$ and the $Ar^+ + H_2$ rovibrational states.

ACKNOWLEDGMENTS

This work was supported by the E. U. Human Capital and Mobility Program through the Structure and Reactivity of Molecular Ions Network under contract number CHRX-CT93-0150. Part of the calculations have been carried out at the ''Institut de Développement et des Ressources en Informatique Scientifique'' (IDRIS). We would like to thank H. Arnout for his contribution in the determination of the prominent part of the decoupled ground adiabatic wave packet in the reaction. Discussions with V. Sidis were of great value to the authors.

[1] W. A. Chupka and M. E. Russell, J. Chem. Phys. **49**, 5426 (1968).
[2] R. M. Bilotta, F. N. Preuninger, and J. M. Farrar, J. Chem. Phys. **73**, 1637 (1980).
[3] K. Tanaka, T. Kato, and I. Koyano, J. Chem. Phys. **75**, 4941 (1981).
[4] (a) F. A. Houle, S. L. Anderson, D. Gerlich, T. Turner and Y. T. Lee, Chem. Phys. Lett. **82**, 392 (1981); (b) J. Chem. Phys. **77**, 748 (1982).
[5] C.-L. Liao, R. Xu, G. D. Flesch, M. Baer, and C. Y. Ng, J. Chem. Phys. **93**, 4818 (1990).
[6] (a) M. Baer and J. A. Beswick, Chem. Phys. Lett. **51**, 360 (1977); (b) Phys. Rev. A **19**, 1559 (1979).
[7] S. Chapman, J. Chem. Phys. **82**, 4033 (1985).
[8] (a) M. Baer, H. Nakamura, and A. Ohsaki, Chem. Phys. Lett. **131**, 468 (1986); (b) M. Baer and H. Nakamura, J. Phys. Chem. **91**, 5503 (1987).
[9] (a) M. Baer, C.-L. Liao, R. Xu, G. D. Flesh, S. Noubarkhsh, C. Y. Ng, and D. Neuhauser, J. Chem. Phys. **93**, 4845 (1990); (b) M. Baer, in *State Selected and State-to-State Ion-Molecule Reaction Dynamics. Part 2: Theory*, edited by M. Baer and C. Y. Ng (Wiley, New York, 1992), pp. 216–236.
[10] M. Gilibert, I. Last, A. Baram, and M. Baer, Chem. Phys. Lett. **221**, 327 (1994).
[11] F. Aguillon, M. Sizun, V. Sidis, G. D. Billing, and N. Marković, J. Chem. Phys. **104**, 4530 (1996).
[12] M. Sizun, F. Aguillon, V. Sidis, V. Zenevich, G. D. Billing, and N. Marković, Chem. Phys. **209**, 327 (1996).
[13] P. J. Kuntz and A. C. Roach, J. Chem. Soc. Faraday Trans. II **68**, 259 (1972).
[14] (a) J. T. Muckerman, R. D. Gilbert, and G. D. Billing, J. Chem. Phys. **88**, 4779 (1988); (b) G. D. Billing and J. T. Muckerman, J. Chem. Phys. **91**, 6830 (1989); (c) N. Marković, G. D. Billing, and J. T. Muckerman, Chem. Phys. Lett. **172**, 509, (1990); (d) N. Marković and G. D. Billing, Chem. Phys. **191**, 247 (1995).
[15] J. C. Tully, J. Chem. Phys. **59**, 5122 (1973).
[16] (a) B. R. Johnson, J. Chem. Phys. **73**, 5051 (1980); (b) J. Chem. Phys. **79**, 1906 (1983); (c) J. Chem. Phys. **79**, 1916 (1983).
[17] N. Marković and G. D. Billing, Chem. Phys. **173**, 385, (1993); N. Marković and G. D. Billing, Chem. Phys. Lett. **248**, 420 (1996); N. Marković and G. D. Billing, Chem. Phys. **209**, 377 (1996).
[18] K. J. McCann and M. R. Flannery, J. Chem. Phys. **63**, 4695 (1975); A. E. De Pristo, J. Chem. Phys. **78**, 1237 (1982); G. D. Billing, Comp. Phys. Rep. **1** (1984).
[19] A. M. Arthurs and A. Dalgarno, Proc. R. Soc. London Ser. A **256**, 540 (1960).
[20] G. D. Billing and N. Marković, J. Chem. Phys. **99**, 2674 (1993).
[21] A. S. Davydov, *Quantum Mechanics* (Pergamon, Oxford, 1965), p. 169.
[22] D. Kosloff and R. Kosloff, J. Comp. Phys. **52**, 35 (1983).
[23] C. Leforestier, R. H. Bisseling, C. Cerjan, M. D. Feit, R. Friesner, A. Guldberg, A. Hammerich, G. Jolicard, W. Karrlein, H-D. Meyer, N. Lipkin, O. Roncero, and R. Kosloff, J. Comp. Phys. **94**, 59 (1991).
[24] H-D. Meyer and W. H. Miller, J. Chem. Phys. **70**, 3214 (1979).